AIP | Review of Scientific Instruments

Review and demonstration of ultra-low-emittance photocathode measurements

Hyeri Lee, Siddharth Karkare, Luca Cultrera, Andrew Kim, and Ivan V. Bazarov

Citation: Review of Scientific Instruments **86**, 073309 (2015); doi: 10.1063/1.4927381
View online: http://dx.doi.org/10.1063/1.4927381
View Table of Contents: http://scitation.aip.org/content/aip/journal/rsi/86/7?ver=pdfcov
Published by the AIP Publishing

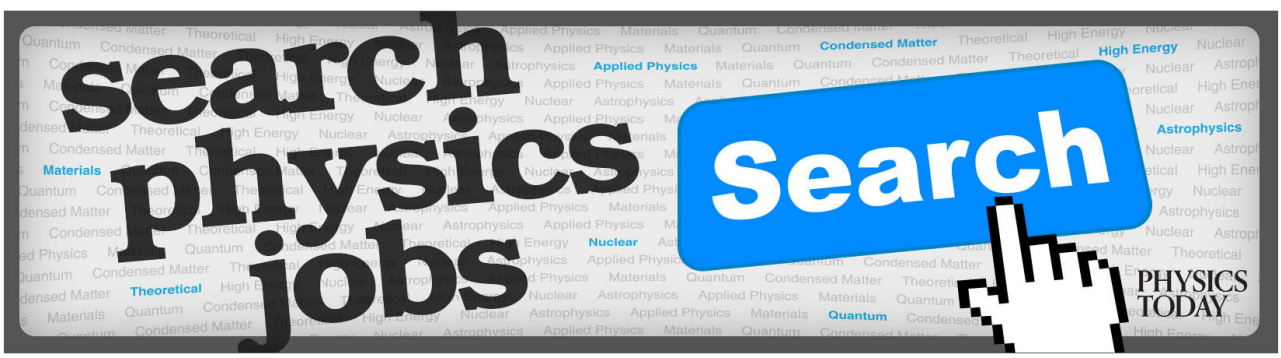

Review and demonstration of ultra-low-emittance photocathode measurements

Hyeri Lee,[a] Siddharth Karkare, Luca Cultrera, Andrew Kim, and Ivan V. Bazarov
CLASSE, Cornell University, Ithaca, New York 14850, USA

(Received 4 May 2015; accepted 14 July 2015; published online 30 July 2015)

This paper reports the development of a simple and reliable apparatus for measuring ultra-low emittance, or equivalently the mean transverse energy from cryogenically cooled photocathodes. The existing methods to measure ultra-low emittance from photocathodes are reviewed. Inspired by the available techniques, we have implemented two complementary methods, the waist scan and voltage scan, in one system giving consistent results. Additionally, this system is capable of measuring the emittance at electric fields comparable to those obtained in DC photoinjectors. © *2015 AIP Publishing LLC.* [http://dx.doi.org/10.1063/1.4927381]

I. INTRODUCTION

The increased electron beam brightness from photocathodes enhances the performance of accelerators and enables new applications[1–4] such as Free electron Lasers (FELs), Energy Recovery Linacs (ERLs), and ultra-fast electron diffraction (UED).[5] Properties like quantum efficiency (QE), mean transverse energy (MTE) or intrinsic emittance, response time, and robustness are important figures of merit to determine the photocathode performance. The maximum possible transverse (two-dimensional) brightness B_n achieved from a photoinjector is determined by the MTE of the photocathode and the electric field at the cathode, E_{cath},[6] and is given by

$$\frac{B_n}{f}\Big|_{max} = \frac{m_e c^2 \epsilon_0 E_{cath}}{2\pi \mathrm{MTE}}, \tag{1}$$

where f is the repetition rate of the beam, m_e is the mass of an electron, c is the speed of light, ϵ_0 is the vacuum permittivity, and MTE of is defined by

$$\mathrm{MTE} = \frac{1}{2} m_e \langle v_\perp^2 \rangle, \tag{2}$$

with the transverse velocity $v_\perp$. In order to maximize the brightness, E_{cath} needs to be maximized and MTE needs to be minimized. As photoinjectors are required to operate at the high cathode field, it is essential to study the electron emission and measure the MTE at various electric fields comparable to the ones in real photoinjectors (several MV/m in DC photoinjectors and up to 100 MV/m in RF photoinjectors).

The MTE can be related to the normalized emittance $\epsilon_{n,x}$ of the beam at the cathode using the expression

$$\epsilon_{\mathrm{n,x}} = \sigma_x \sqrt{\frac{\mathrm{MTE}}{m_e c^2}}, \tag{3}$$

where σ_x is the rms size of the illuminated spot on the cathode[7] when there is no correlation between the position and the momentum on the phase space.

The MTE has been characterized experimentally[3,7–9] and theoretically[10,11] for various photocathodes. However, photocathodes with MTE below 100 meV have not been routinely studied and the corresponding physics mechanisms oftentimes remain poorly understood. We aim to build a simple and reliable tool to measure low MTE (below 100 meV) or equivalently, ultra-low emittance (<0.4 mm-mrad per mm rms laser spot) at photoinjector-comparable electric fields and at cryogenic temperatures.

The organization of the paper is as follows. We first review and compare the available methods for measuring very low MTE electron beams. We then provide a detailed description of a device called the Transverse Energy Meter (TEmeter) developed at Cornell University photocathode laboratory to measure very low MTEs with two methods, the waist scan and the voltage scan. This design supports cooling of the photocathode from room temperature (300 K) to cryogenic temperatures (90 K). We also present a detailed systematic error analysis, which is essential in order to build reliable measurement apparatus. Finally, using the TEmeter, we demonstrate the measurement of electron beams with MTEs as low as 22 ± 1 meV from a cryo-cooled alkali antimony cathode.

II. REVIEW OF LOW EMITTANCE MEASUREMENT SYSTEMS

In this section, the review and comparison between currently available methods to measure very low MTE are discussed. Table I summarizes main available techniques.

The transverse energy spread can be inferred using hemispherical analyzers[12,13] as well as time of flight (TOF) based detectors[14,15] in Angle Resolved Photoemission Spectroscopy (ARPES) experiments. Fig. 1 shows a typical experimental configuration with a hemispherical analyzer.[12] Light with a photon energy larger than the work function of the material is incident on its surface. The emitted electrons are then collected by the hemispherical/TOF analyzer to give their energy and azimuthal/polar angular distributions. By rotating the sample stage, electrons from all angles can be obtained.[15] Such analyzers are designed to study the energy-momentum dispersion

[a]Electronic mail: HL823@cornell.edu

TABLE I. Comparison of existing methods.

Method	Configuration	Disadvantage	Lowest MTE measured
Hemispherical analyzer[12]	Differential voltage applied to sort energies	(1) Sensitive to work function differences at low energies (2) Not a direct measurement for emittance (3) Sensitive to stray E/B fields (4) Unreliable when measuring kinetic energy below 1eV (5) Cannot measure at fields greater than few V/m	~100 meV[13]
TOF analyzer[14,15]	Delayed line detector to measure TOF and transverse position	(1) A sub-ps laser pulse necessary (2) Sensitive to stray E/B fields (3) Unreliable when measuring kinetic energy below 1eV (4) Cannot measure at fields greater than few V/m	~130 ± 5 meV[15]
Energy analyzer[16,17]	Motion of electrons in longitudinal magnetic field	(1) Cannot measure at fields greater than few V/m (2) Strong magnetic field might affect photoemission	25 ± 2.5 meV
E × B technique[18,19]	Crossed electric and magnetic field between the plates	Impractical to extract MTE information due to complex mathematical post-processing involved	N/A
Waist scan[3,7,20–22]	Electron gun + a magnetic lens	Careful magnetic field calibration required	~1 meV[3]
Beam sampling/ pepper-pot[21,23,24]	Two slits + a detector/a slit + a detector	Resolution comparable to the intrinsic emittance for low MTE beams	35 meV[25]
Free expansion[26]	Acceleration + free expansion	(1) Laser diffraction (2) Small laser spot required (3) Grid non-uniformity	27 meV[26]
TESS[27]	Free expansion in acceleration	(1) Small laser spot required (2) Cannot measure at fields greater than few kV/m	45 ± 7 meV[27]

relationship in solids[12] and can map energy and angular distribution of emitted electrons from which it is possible to infer the MTE. The main issue to measure the low MTE electrons is that the analyzer is designed to deal with electrons emitted with a kinetic energy larger than a few eV. This limitation arises from the sensitivity of low energy electrons to stray magnetic fields and work function differences between the analyzer and the cathode. This limits the usefulness of these systems to studying the emission processes for higher (>eV) energy electrons.

Several other techniques exist to measure the MTE of low energy electrons by using strong electric or magnetic fields. Longitudinal and transverse energy distributions can be measured using the principle of adiabatic invariance and the motion of low energy electrons in a strong magnetic field.[16,17] The configuration is shown in Fig. 2. A resolution of less than 6 meV rms in the energy distributions was demonstrated by this method.[16] The MTE of as low as 25 ± 2.5 meV has been measured from GaAs photocathodes using this technique. However, this technique does not allow measurement of MTE under high electric fields. Thus, it cannot reproduce the conditions in an actual photoinjector and measure the dependence of MTE on the electric field. In addition to that, it is not understood how strong magnetic fields used in this setup would affect photoemission processes with ultra-low MTE.

Another method to measure a complete 3-D energy distribution by using crossed electric and magnetic fields was proposed.[18] However, retrieving the actual distribution from the measured photocurrents requires the use of complex Radon transforms,[18] which is not practical. Due to this mathematical complexity, only 1-D distributions of polar angle and

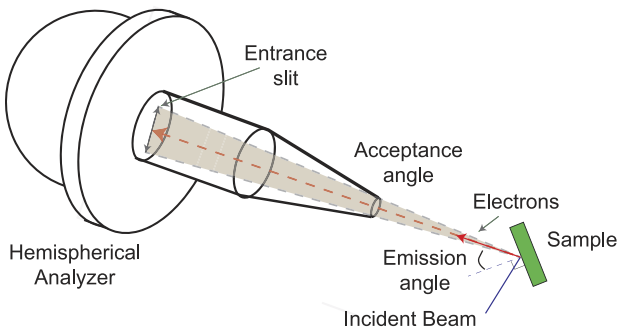

FIG. 1. Hemispherical analyzer schematic for ARPES.[12]

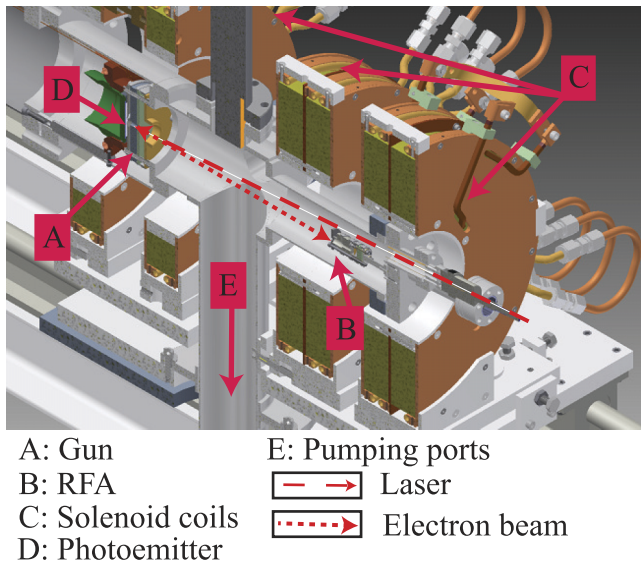

FIG. 2. A section view of 2D energy analyzer. RFA is a acronym of retarding field analyzer. The details can be obtained in Ref. 16.

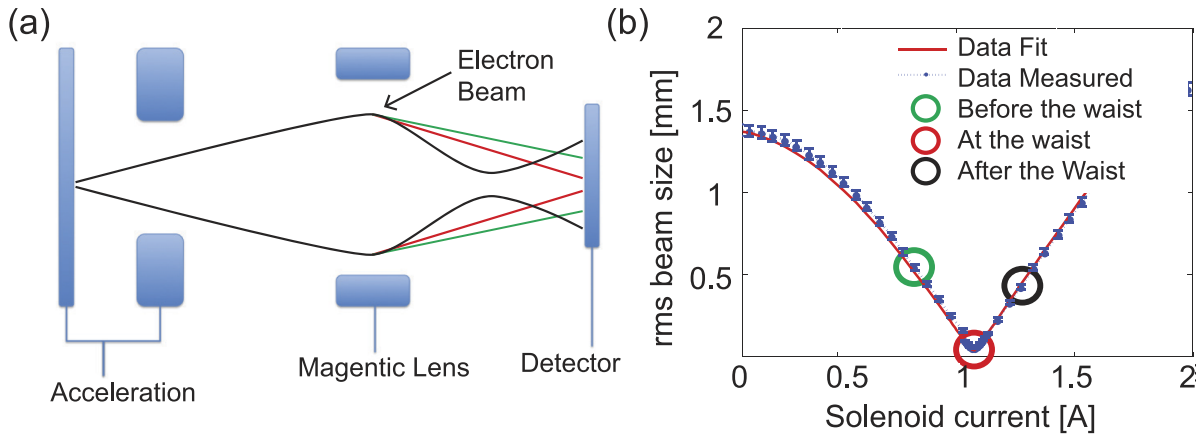

FIG. 3. (a) Configuration of the waist scan. The magnetic lens has a variable focal length. The black, red, and green lines represent the cases when the waist is before, at, and after the scintillator screen respectively. The final rms beam sizes are measured as the current of the magnetic lens varies as shown in (b). The emittance is obtained from the least square fit based on the transport matrix. Each line in (a) corresponds to the colored circles in (b).

longitudinal energy have been separately obtained.[19] Hence, this technique is not useful to measure the MTE.

Waist (or solenoid/quad) scan is one of the simplest and most common ways to measure the MTE in photoinjectors. This involves a magnetic lens such as a solenoid or a quadrupole, located in a drift region after an acceleration by an electric field. The schematic of the configuration is shown in Fig. 3(a). The electric field accelerates the electron beam to a relatively high energy. The focal length of the magnetic lens is varied by changing its current. This changes the electron beam envelope accordingly. The rms beam size at a certain distance away from the magnetic lens is measured using scintillator screen followed by a charged-coupled device (CCD) camera. For a particular electron energy, the spot size on the scintillator screen is recorded as a function of the current in the magnetic lens. The emittance of the beam at the photocathode and hence the MTE can be deduced from these measurements if the linear transport matrices of the accelerating field and the focusing lens are known. When all the beam transport elements (accelerating field and the magnetic lens) behave linearly, the electron trajectories can be modeled using a method similar to optical ray tracking. The linear transfer matrices $\mathbf{R} = \mathbf{R}_{i\to f}$ connect the initial profile of the beam at the photocathode to the final profile on the scintillator screen as follows:

$$\begin{pmatrix} \sigma_x \\ \sigma_{\theta_x} \end{pmatrix}_f = \mathbf{R} \begin{pmatrix} \sigma_x \\ \sigma_{\theta_x} \end{pmatrix}_i, \tag{4}$$

where the beam profile consists of its rms beam size, σ_x, and divergence, σ_{θ_x}.[28] Detailed description about how to obtain the MTE from the spot size measurements can be found elsewhere.[7,20] Various Refs. 3, 7, and 20–22 have shown studies of emittance measurements from diverse electron sources such as metal[22] and semiconductor photocathodes[7,20] and ionized electrons trapped in a magneto-optical trap (MOT).[3] Since this method strongly depends on the transport matrices and final beam sizes, extra attention needs to be paid to the precise modeling of each of the beam elements, nonlinear effects, and the accuracy of the beam sizes. Exact measurements of the distances between the cathode, the anode, the focusing magnetic lens and scintillator screen, and the electric and magnetic fields of the elements are necessary. Additionally, nonlinear effects such as aberrations and the space charge make it difficult to properly model this method and may even preclude its proper use. High resolution of detector and the CCD camera is also required.

Another popular way to measure the MTE in photoinjectors is a pepper pot or a beam sampling technique.[23] The main advantage of beam sampling is that it allows mapping of the transverse phase space. In this method, two slits are placed in the electron beam path to sample the beam where the slits are thick enough to stop the beam. The current of the beam so sampled is recorded. A schematic of this method is shown in Fig. 4. The first slit with the width d_1 selects the electron beam at the transverse position x away from the center of the beam. The selected electrons are then allowed to pass through a drift region. In the drift region, these electrons expand freely according to their transverse momentum spreads. The second slit with width d_2 is placed at the end of the drift region and only a few electrons which pass through the second slit are measured by a Faraday cup.[24] In order to obtain the entire phase space, scanner coils are used to sample the beam at various positions and transverse momenta. For a given energy of the beam, the resolution for this technique is limited by width of the two slits and the distance between them. Another variation of this method includes using one slit or a grid of small holes (called a "pepper pot"), and a screen instead of

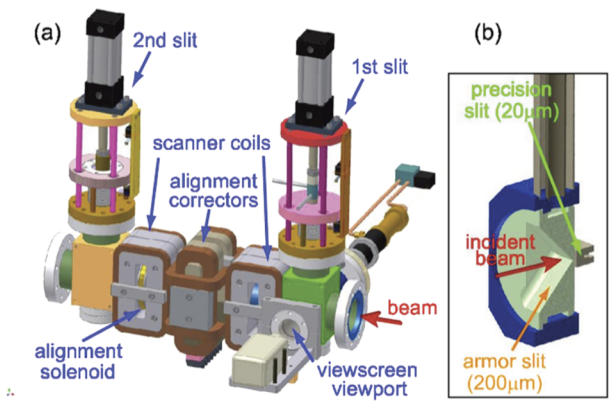

FIG. 4. Two-slit emittance measurement system.[29]

two slits.[21,30] It is also possible to measure a time resolved phase-space by using a deflecting cavity in place of the Faraday cup.[31] At high energies, the slit becomes too thick so that it restricts the range of angles and also offers more opportunity to scatter. Although this method can map the entire transverse phase space and determine the emittance, the resolution of the phase space measurement can be comparable to the emittance obtained from the ultra-low MTE photocathodes making this technique inappropriate for the ultra-low emittance. Furthermore, this method inevitably involves interaction between slits and an electron beam. The contact of the electron beam with the slits can scatter the electrons and affect the MTE. While this effect may not be significant for the higher energy beam with a high MTE, it is not well understood how this method will affect a very low MTE beam.

The simplest method by far is to allow the beam to expand freely in an acceleration and a drift region and obtain the MTE or the transverse energy distributions from the transverse size of the beam after the expansion.[26,27] As shown in Fig. 5, an electron beam is generated from a small spot on the cathode (<100 μm rms) using a focused laser. The electrons emitted experience a high gradient electric field between the cathode and the anode which is a fine electron microscope grid parallel to the cathode. The anode grid opening is small so that the defocusing due to the grid opening is negligible compared to the low MTE. The electron beam is accelerated only along its propagation direction. It passes through the grid and travels in a drift region to the scintillator screen where it is imaged. In the drift region, the electron beam expands due to the transverse velocities of the electrons. The scintillator screen along with the micro-channel plate (MCP) and a CCD camera obtains the image of the beam. The spot size on the scintillator screen is a function of the initial transverse energy of the beam, the voltage applied, a gap between the cathode and anode, and the distance of the drift region.[26] Despite the simplicity of this technique, much care is required to ensure that the grid does not contribute to the measured MTE. The details regarding the grid contribution to systematic errors are given in Appendix A.

A variation of this configuration called transverse energy spread spectrometer (TESS) allows the beam to expand up to the anode. Instead of a grid, the anode consists of the MCP and the scintillator screen. The beam spot is recorded on the anode itself.[27] Given the voltage and the distance between the anode and the cathode, the image of the beam spread can be converted into the transverse momentum distribution and the MTE. This technique requires using a low (~100 V) voltage between the cathode and the anode in order to obtain a big enough spot size on the cathode. Hence, this techniques is incapable of measuring MTE at high electric field gradients.

This review shows the advantages and disadvantages of each method. Considering the goal of measuring the low MTE from the photocathodes at photoinjector-comparable electric fields, the waist scan and the free expansion method are the simplest and the most reliable. The hemispherical analyzer, TOF spectroscopy, and 2-D analyzer are unable to provide the MTE measurement at various electric fields, and the crossed electric and magnetic field analyzer is only able to give the angular and longitudinal distribution of the emitted electrons. A pepper pot/beam sampling technique is limited by a spatial and momentum resolution from the configurations of the system.

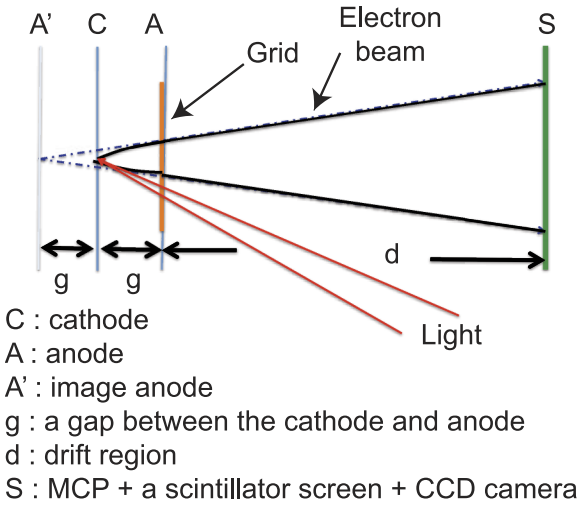

FIG. 5. A schematic of free expansion technique.[26]

III. DEMONSTRATION OF CORNELL ULTRA-LOW EMITTANCE MEASUREMENT

This section describes a system dedicated to measuring the ultra-low emittance of photocathodes with MTE below 100 meV. It includes the detailed description of the setup, measurement methods, analysis for error sources, and the results.

A. Description of TEmeter

The setup has been developed at the Cornell University Photocathode Lab and called the TEmeter. The photogun in TEmeter is capable of providing an electric field up to 3MV/m with a maximum voltage of 20 kV. The system also has a cryogenic system which cools the photocathode down to 90 K. The schematic is shown in Fig. 6.

The cathode holder stays on top of a thermal reservoir made of a copper block, which can be cooled by liquid nitrogen (LN). The temperature of the cathode surface reaches 90 K in 2 h once the copper reservoir is full of liquid nitrogen.

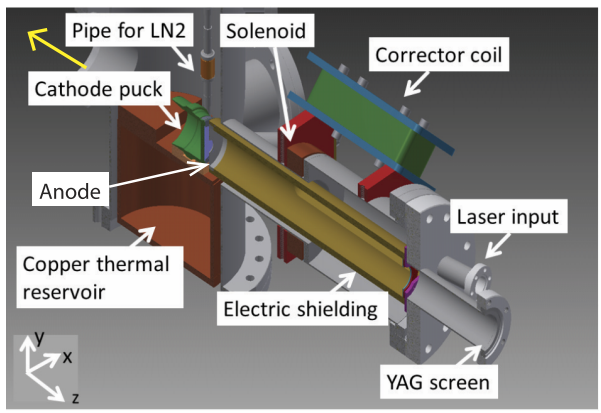

FIG. 6. TEmeter chamber and beam line used in ultra-low emittance measurement. The beam moves toward positive z direction. The growth chamber is connected from negative z direction as the yellow arrow points out.

The TEmeter is connected to an alkali antimonide growth chamber via a UHV connection system with pressure in the sub 10^{-10} Torr range.[32] Alkali antimonide cathodes are grown on Si substrates on a circular stainless steel or molybdenum puck with 1 in. diameter in the growth chamber and transferred into the TEmeter. The vacuum in the TEmeter is 2×10^{-10} Torr.

The cathode along with the nitrogen reservoir is biased to a negative voltage while the anode is grounded. The cathode holder is designed so that the gap between the cathode and anode is approximately 5 mm. The exact gap can vary by ±1 mm every time the cathode is inserted into the system. Therefore, the gap is measured each time to determine the appropriate electric field map. The anode has a hole of 12 mm diameter and is held by a cylindrical electric field shield in order to minimize the stray electric field after the anode. Light passes through a pinhole, which is 1:1 imaged on the cathode using a set of convex lenses through an UHV window with about 6° angle with respect to the axis of the electron gun. The pinhole can be illuminated using a laser or the light from a monochromator. The photocurrent remains low to avoid the space charge effects.

In the drift region, there is a solenoid and two sets of corrector coils. The corrector coils are used to cancel the effects of stray magnetic fields, including the earth's magnetic field, and to center the beam on the YAG screen. The corrector coils are wired in an aluminum mount and attached to the beam line.

The beam size on the YAG screen is measured by a CCD camera connected to a computer. The CCD camera zooms in on the screen using a telescope so that a 11 μm/pixel resolution can be obtained. The initial beam size is measured using the telescope with a resolution of 27 μm/pixel. The beam size on the cathode used the experiments are 60, 140, and 170 μm which will be discussed in detail in Sec. III C.

B. Measurement methods

1. The waist scan

The waist scan follows the same principle as described in Refs. 7 and 20. It is important to remember that the waist scan method strongly depends on its measured rms beam sizes, especially sensitive near the beam waist. In this setup, the final beam size varies from 1 mm to 10 μm; however, due to the limited CCD pixel size, it is difficult to operate with one resolution to measure large variation of the beam sizes. This leads to taking the measurements with two different resolutions. The low resolution (~50 μm/pixel) captures the beam away from the waist and high resolution (~10 μm/pixel) measures the beam near the waist. When data taken by low and high resolution are combined, the most accurate emittance value can be obtained. Fig. 7 shows how combined resolution measurement produces the complete data set.

2. Voltage scan

This configuration does not rely on the solenoid and is close to the one for free expansion as mentioned before. The main difference between free expansion and voltage scan is the way each method obtains the emittance and MTE values. The free expansion converts the beam distribution on the screen at a given fixed voltage to the momentum in order to get the emittance and MTE. However, the voltage scan deduces the emittance from measurements of the rms beam size on the YAG screen at various voltages as shown in Fig. 8. The linear transport matrices can be constructed for the electric field generated by the cathode-anode configuration. This can be used to obtain the MTE from the rms beam size vs anode voltage curve using a least square fit as done in the waist scan method.

C. Error consideration for the TEmeter

In this section, we discuss possible sources of errors in the MTE measurement described above. SUPERFISH[33] is used to generate the electric and magnetic field maps in the TEmeter, and the General Particle Tracer (GPT)[34] is used to simulate the beam line of the TEmeter for both the waist scan and voltage scan configurations.

In the absence of space charge effects and non-linear beamline elements, the intrinsic emittance $\epsilon_{intrinsic}$ is preserved along the beam line. The beam current used for the

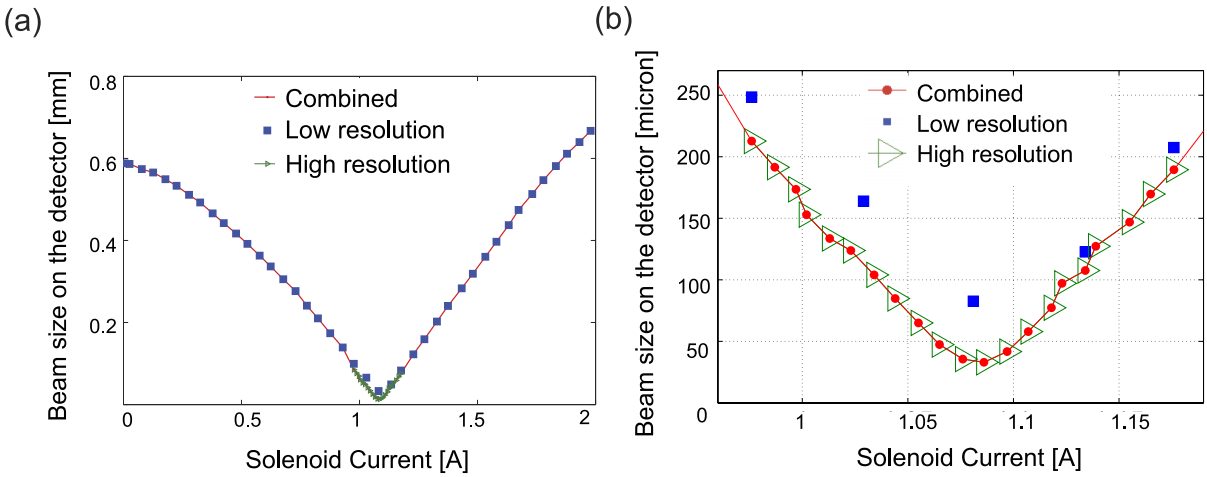

FIG. 7. The solenoid scan works best when data from two different resolutions (11 μm/pixel and 45 μm/pixel) are combined. Figure (a) compares the data set for all resolutions. Figure (b) shows how high resolution captures its beam waist.

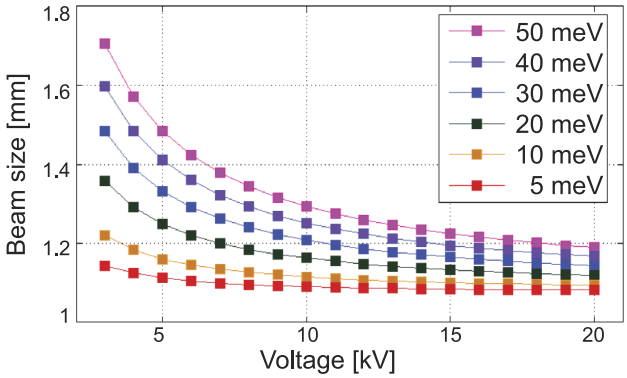

FIG. 8. The rms beam size on the screen with respect to its beam energy for its initial MTE as obtained from GPT simulations. The rms beam size on the cathode is 60 μm.

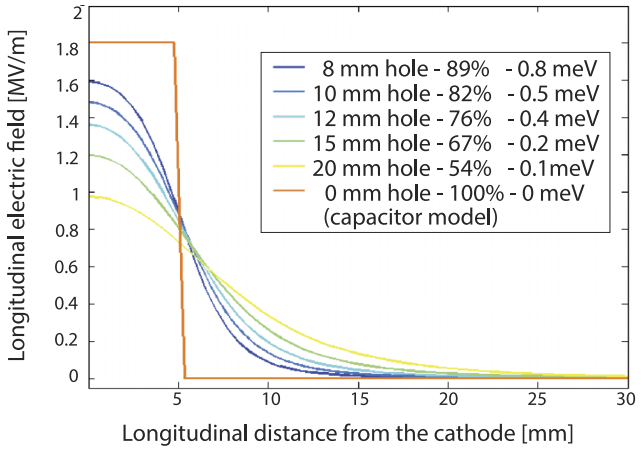

FIG. 9. This figure shows the longitudinal electric fields for various hole sizes and relative field strength compared to the field for the capacitor model by using SUPERFISH.[33] It also provides the MTE gain for 500 μm initial beam on the cathode and zero intrinsic emittance.

measurement in the TEmeter is small enough that space charge is not an issue. However, non-linearity in the anode and solenoid fields needs consideration. The emittance growth due to the non-linear fields can be assumed to be uncorrelated and the total measured emittance can be given by

$$\epsilon_{total} = \sqrt{\epsilon^2_{intrinsic} + \epsilon^2_E + \epsilon^2_B + \epsilon^2_{B_{cath}} + \epsilon^2_{others}}, \quad (5)$$

where ϵ_E is the emittance growth due to the electric field aberration, ϵ_B is due to the magnetic field aberration, $\epsilon_{B_{cath}}$ is due to the magnetic field on the cathode, and ϵ_{others} due to other factors like limited resolution while measuring the beam spot and mechanical vibration.

1. Electric field aberration

The emittance growth due to the electric field aberration results from two main sources: an anode hole and a stray field. With proper design, the effects of the stray fields can be minimized and ignored. The details regarding this are given in Appendix B.

In order to minimize the anode hole contribution, an optimization of the anode hole size is required. A SUPERFISH[33] simulation is performed to calculate electric fields along the propagation axis and the MTE gain due to the emittance growth from the resulting aberration, see Fig. 9. As the hole size increases, the emittance growth due to the anode aberration decreases; however, the electric field at the cathode also decreases. The emittance growth due to anode aberrations also increases with the size of the spot on the cathode and its offset from the center. In order to maintain the emittance growth below 5% for a initial spot size smaller than 200 μm and an offset of less that 100 μm and obtain a strong enough electric field at the cathode, the anode hole size was chosen to be 12 mm in diameter.

2. Magnetic field aberration

The emittance growth due to the solenoid aberration can be calculated by

$$\epsilon_B = \frac{2\alpha\sigma^3_{xs}}{\beta\gamma}\sqrt{5x_0^2 + 2\sigma^2_{xs}}, \quad (6)$$

where x_0 is the beam offset from the solenoid magnetic axis, σ_{xs} is the beam size in the solenoid, and α is defined by

$$\alpha = \frac{1}{4}\left(\frac{e}{2m_e c\beta\gamma}\right)^2 \int \left(\frac{\partial B}{\partial z}\right)^2 \mathrm{d}z. \quad (7)$$

Here, β and γ are the relativistic factors.[35] Since the emittance growth is proportional to the 4th power of σ_{xs}, we use the smallest possible laser spot on the cathode. There may be an offset of up to 3 mm between the anode and the solenoid due to the mechanical design of the setup. With this offset and a MTE of less than 50 meV, the beam size at the cathode should be smaller than 60 μm to keep the emittance growth below 5%.

3. Magnetic field on the cathode

When the electron beam is emitted from a cathode with a nonzero residual field B_z, it obtains an angular velocity that leads to emittance growth. The transverse momentum then becomes $\sigma_{p_\perp} = \gamma m \sigma_x \dot{\theta}$, where $\dot{\theta} = -\frac{eB_z}{2\gamma m}$. Since $\epsilon_{n,x} \sim \frac{\sigma_{p_\perp}}{mc}\sigma_x$, the growth is estimated by

$$\epsilon_{B_{cath}}[\mathrm{mm-mrad}] \sim 0.3 B_z[\mathrm{mT}]\sigma_x^2[\mathrm{mm}], \quad (8)$$

where σ_x is the spot size on the cathode.[23] The magnetic field at the cathode is 0.23 mT when the solenoid current is set to 1 A. As the gun voltage increases to above 10 kV, the solenoid current for its waist gets larger than 2 A, and the solenoid for measurement ranges up to 3 A. As shown in Fig. 10, the initial beam size on the cathode must be approximately 60 μm in order to avoid the emittance growth becoming greater than 5%.

4. Other possible error sources

Inaccurate measurement of the rms beam size on the scintillator screen will contribute to systematic errors in MTE. According to GPT simulations, the waist size goes below 20 μm for a MTE of ~30 meV for the voltage of 10 kV. A

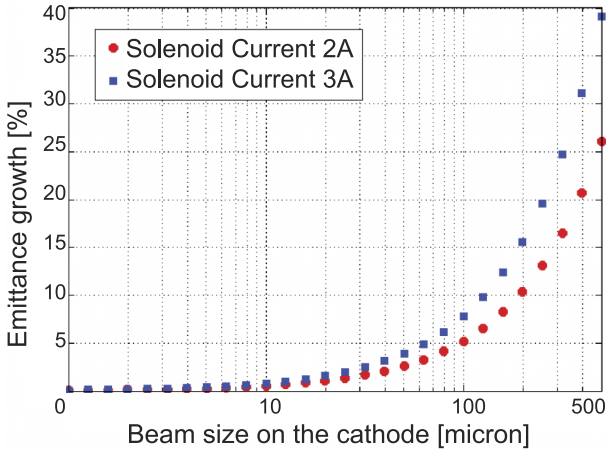

FIG. 10. Emittance growth according to the initial beam sizes and solenoid currents with respect to its cathode intrinsic emittance for 30 meV as obtained from GPT simulations.

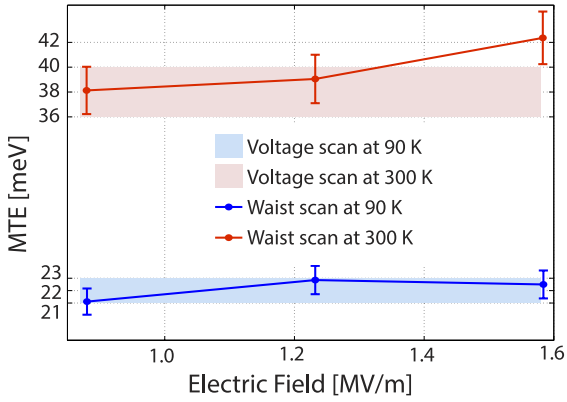

FIG. 11. The MTE results obtained at 90 K and 300 K for the solenoid scan and voltage scan. The electric field intensities at the cathode surface for the voltage scan vary between 0.5 and 3.4 MV/m.

resolution of 11.3 μm/pixel is sufficient to measure this spot accurately. However, a better resolution will be required to measure smaller spot sizes. In order to maintain the spot size above 20 μm rms, the voltage during the solenoid scan was kept below 10 kV.

These methods depend strongly on the final rms beam sizes, so the reliability of the sizes on the detector is important. With high currents, there is a possibility of saturation on the screen. When the electrons charge up the screen, the final beams may be distorted, negatively affecting the measurement. Another consideration is the thickness of the scintillator. A thicker scintillator can increase the amount of light produced but also add blurring. Instead, a MCP can be helpful for the very low current operation. It is necessary to ensure that the scintillator screen or MCP has a uniform sensitivity.

One should be aware that mechanical vibrations can contribute to the errors. The accurately measured beam sizes are a key requirement of this configuration. The spectrum of the vibrations is unknown and it is non-trivial to quantify the effect of vibrations and subtract its effect, particularly when the beam is tightly focused at its waist.

5. Requirements for measurements

The goal is to avoid having an emittance growth greater than 5% or having a systematic error in the MTE of 10%. For the voltage scan, the aberration due to the hole is negligible when the beam size at the cathode is smaller than 200 μm with an offset of 100 μm.

To limit the effect of magnetic field aberrations on waist scans, the rms beam size at the cathode must be less than 100 μm. In addition, the emittance growth due to the magnetic field on the cathode limits the beam size at the cathode to 60 μm and requires operating with solenoid currents less than 2 A. These requirements lead to operating voltages below 10 kV and an initial beam size of 60 μm.

D. The result

We performed the ultra-low emittance measurements with both methods described above using a Cs_3Sb photocathode grown by co-deposition of Sb and Cs. For the solenoid scan with an rms beam size at the cathode of 60 μm, the voltage was kept below 10 kV (equivalent to a 1.6 MV/m electric field at the cathode).

The results obtained from the solenoid scan was found to be independent of the electric field at the cathode Fig. 11. This figure also shows that the MTE reduction from the ambient temperature (300 K) to the cryogenic temperature of 90 K. The voltage scan could be performed.

Since the MTE obtained from the solenoid scan was found to be independent of the electric field at the cathode, the voltage scan could be performed to confirm the results obtained by the solenoid scan. Voltage scans with three different rms beam sizes (60, 140, and 170 μm) were also performed to obtain the same MTE as the solenoid scan. At the cryogenic temperature of 90 K, the MTE of 22 ± 1 meV was measured. The details of these results are in Ref. 36.

IV. SUMMARY

A compact device (TEmeter) that incorporates two independent techniques (the waist scan and the voltage scan) to measure low MTEs from photocathodes was developed. The TEmeter can not only measure photocathode MTE at high electric fields (comparable to those found in photoinjectors) but also measure MTE from cryogenically cooled photocathodes. The excellent agreement between the two techniques reinforces the validity of this measurement especially at small MTEs. It is possible to connect this tool to photocathode growth systems making it easy to characterize photocathodes and study photoemission physics under high electric fields.

ACKNOWLEDGMENTS

This work has been funded by the National Science Foundation (Grant No. PHY-1416318). The authors would like to acknowledge the efforts of Dr. Xianghong Liu for the mechanical design of the TEmeter.

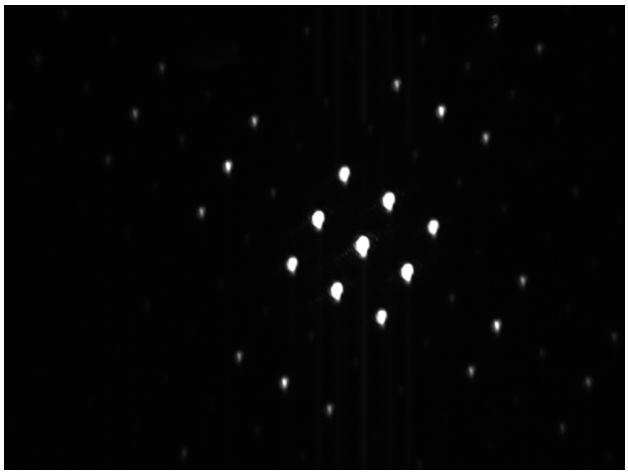

FIG. 12. A diffraction pattern with 473 nm laser. This image is taken 5 mm away from the grid. A minimum distance between patterns is 250 μm.

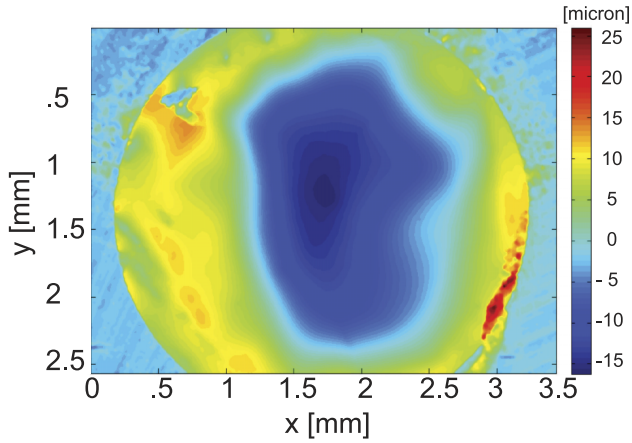

FIG. 14. The grid deformation. This is obtained from a darkfield light microscope.

APPENDIX A: SOURCES OF SYSTEMATIC ERRORS OF FREE EXPANSION METHOD

In this appendix, we describe the issues encountered while implementing this free expansion technique which affects the accuracy of the method.

1. Diffraction on the cathode due to the grid

The grid in the anode plays a key role in providing the constant longitudinal electric field while generating no transverse field. However, one issue is that the grid is in the path of the illuminated laser. When the tightly focused laser passes through the grid, it forms a diffraction pattern making the effective spot size larger thus introducing an uncertainty in the MTE measurement.

The diffraction pattern due to the grid (of 12.5 μm spacing) at a distance of 5 mm away with 473 nm laser is shown in Fig. 12. We simulated the free expansion technique by using the diffraction pattern as a source instead of the focused spot. The results are shown in Fig. 13. The effect shows the significant electric field dependence on the low MTEs. The distance between the diffraction spots depends on the wavelength of the laser and grid spacing. Hence, it may be possible to avoid this problem by using a bigger grid spacing. The bigger grid spacing may, however, introduce errors related to the focusing from the grid.[26]

To avoid this problem, we replaced the grid holder with a glass anode coated with 50 Å titanium and allowing the laser to pass through the glass instead of the grid.

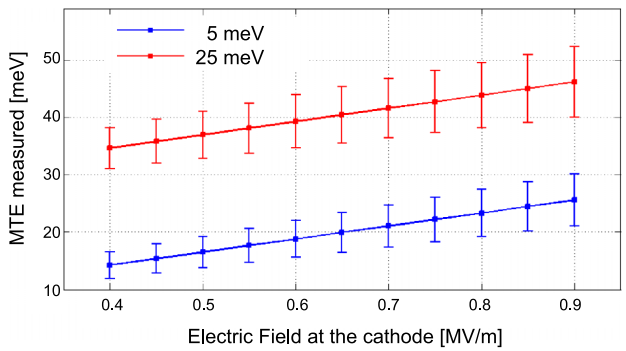

FIG. 13. A diffraction pattern contributes to incorrect MTE measurements. When the initial MTE is given as shown in the legend, the MTE measured shows the electric field dependence.

2. Grid non-uniformity

The commercially available grid is thin (10 μm in our case) and gets easily deformed. Fig. 14 shows the non-uniformity in the flatness of the grid due to the deformation. The free expansion setup in Ref. 26 avoided this issue by implementing a stretched electroformed grid, but such a grid is not compatible with the glass anode holder used in the TEmeter. While this non-uniformity exists in the setup, it is difficult to model the exact electric fields in the acceleration region, resulting in the non-uniform grid contributing to an uncertainty in the results.

To ensure an accurate measurement and a small uncertainty, we decided to use an anode with a hole instead of a grid. This enabled us to simulate the setup accurately without having to deal with the uncertainties involved in the grid non-uniformity.

APPENDIX B: STRAY ELECTRIC FIELD

The way the anode and the cathode are supported can change the stray field. In our original design, the anode was located on top of the thermal reservoir held by insulators as shown in Fig. 15(a). This leads to stray fields in the drift region several cm around the anode. These electric fields were sufficient to cause noticeable emittance growth and lead to erroneous MTE measurements.

To overcome this issue, the support for the anode was changed. In the new design, the anode was supported by a grounded cylinder that enclosed the drift space beyond the anode and blocked out any stray fields. The new design is shown is Fig. 15(b).

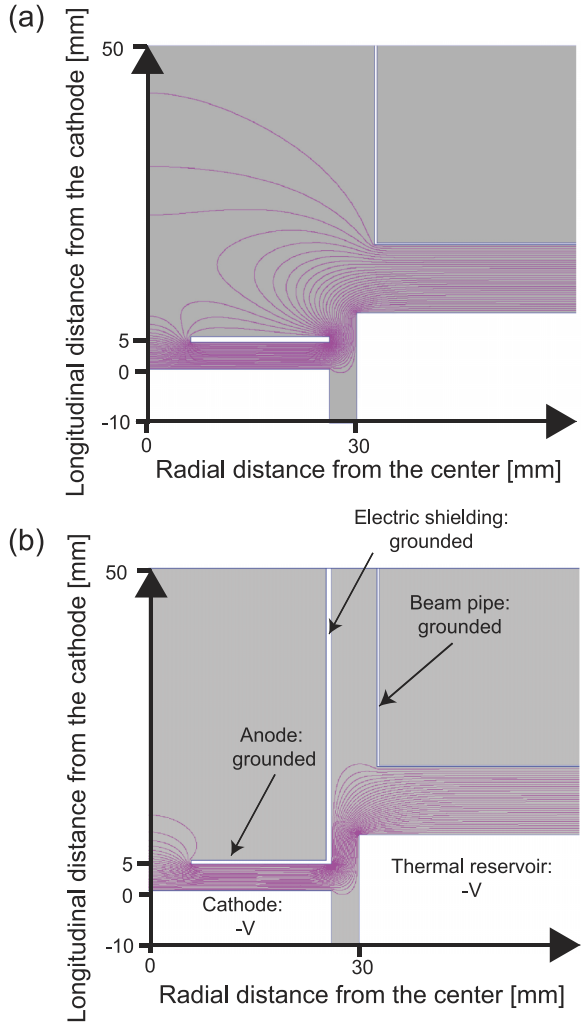

FIG. 15. Comparison between two configuration: (a) shows the electric field line (purple line) without the electric shield and (b) shows the line with the shield (the grounded cylinder).

[1]I. Ben-Zvi *et al.*, Nucl. Instrum. Methods Phys. Res., Sect. A **532**, 177 (2004).
[2]S. M. Gruner *et al.*, Rev. Sci. Instrum. **73**, 1402 (2002).
[3]W. J. Engelen *et al.*, Ultramicroscopy **136**, 73 (2014).
[4]U. J. Lorenz and A. H. Zewail, Science **344**, 1496 (2014).
[5]J. R. Dwyer *et al.*, Philos. Trans. R. Soc., A **364**, 741 (2006).
[6]I. V. Bazarov *et al.*, Phys. Rev. Lett. **102**, 104801 (2009).
[7]I. V. Bazarov *et al.*, J. Appl. Phys. **103**, 054901 (2008).
[8]D. H. Dowell and J. F. Schmerge, Phys. Rev. Spec. Top.–Accel. Beams **12**, 074201 (2009).
[9]H. J. Qian *et al.*, Phys. Rev. Spec. Top.–Accel. Beams **15**, 040102 (2012).
[10]S. Karkare *et al.*, J. Appl. Phys. **113**, 104904 (2013).
[11]S. Karkare and I. Bazarov, Appl. Phys. Lett. **98**, 094104 (2011).
[12]A. D. Palczewski, "Angle-resolved photoemission spectroscopy (ARPES) studies of cuprate superconductors," Ph.D. thesis, Iowa State University, 2010.
[13]T. C. Droubay *et al.*, Phys. Rev. Lett. **112**, 067601 (2014).
[14]Y. Wang, "Laser-based angle-resolved photoemission spectroscopy of topological insulators," Ph.D. thesis, Harvard University, 2012.
[15]D. Sertore *et al.*, in *Proceedings of European Particle Accelerator Conference EPAC 2004* (European Physical Society Accelerator Group (EPS-AG), Lucerne, Switzerland, 2004).
[16]S. Karkare *et al.*, Rev. Sci. Instrum. **86**, 033301 (2015).
[17]D. A. Orlov, M. Hoppe, U. Weigel, D. Schwalm, A. S. Terekhov, and A. Wolf, Appl. Phys. Lett. **78**, 2721 (2001).
[18]V. E. Andreev, A. L. Bukhgeim, and A. S. Terekhov, J. Inverse Ill-Posed Probl. **7**, 427 (1999).
[19]V. V. Bakin *et al.*, J. Exp. Theor. Phys. Lett. **77**, 167 (2003).
[20]I. Bazarov *et al.*, Appl. Phys. Lett. **98**, 224101 (2011).
[21]S. G. Anderson, J. B. Rosenzweig, G. P. LeSage, and J. K. Crane, Phys. Rev. Spec. Top.–Accel. Beams **5**, 014201 (2002).
[22]C. P. Hauri *et al.*, Phys. Rev. Lett. **104**, 234802 (2010).
[23]M. Reiser, *Theory and Design of Charged Particle Beams* (Wiley, New York, 1994).
[24]C. Gulliford *et al.*, Phys. Rev. Spec. Top.–Accel. Beams **16**, 073401 (2013).
[25]J. Maxson *et al.*, Appl. Phys. Lett. **106**, 234102 (2015).
[26]J. Feng, J. Nasiatka, W. Wan, T. Vecchione, and H. A. Padmore, Rev. Sci. Instrum. **86**, 015103 (2015).
[27]L. B. Jones *et al.*, *Proceedings of Free-Electron Laser FEL2013, Vol. FEL Technology 1* (Joint Accelerator Conferences Website (JACoW), New York, NY, USA, 2013).
[28]M. G. Minty and F. Zimmerman, *Measurement and Control of Charged Particle Beams* (Springer, New York, 2003).
[29]I. V. Bazarov *et al.*, Phys. Rev. Spec. Top.–Accel. Beams **11**, 100703 (2008).
[30]R. K. Li *et al.*, Phys. Rev. Spec. Top.–Accel. Beams **15**, 090702 (2012).
[31]H. Li, "Multi-dimensional characterization of the laser and electron beams of the Cornell energy recovery linac photoinjector prototype," Ph.D. thesis, Cornell University, 2012.
[32]L. Cultrera *et al.*, in *Proceedings of International Particle Accelerator Conference IPAC2012* (IPAC'12 OC, New Orleans, Louisiana, USA, 2012).
[33]Los Alamos National Laboratory, "Poisson Superfish," http://laacg.lanl.gov/laacg/services/download_sf.phtml.
[34]Pulsar Physics, "General particle tracer (gp)," http://www.pulsar.nl/gpt/.
[35]I. V. Bazarov *et al.*, Phys. Rev. Spec. Top.–Accel. Beams **14**, 072001 (2011).
[36]L. Cultrera, S. Karkare, H. Lee, X. Liu, and I. Bazarov, e-print arXiv:1504.05920.